E-20-F29
#3

Final Report

NASA Research Grant NAG5-8658
Georgia Tech Research Corporation
Georgia Institute of Technology

Period of Performance: 15-Aug-1999 through 30-September-2002

Quantifying the Relationship Between Remotely-Sensed and Modeled Soil Moisture

C. D. Peters-Lidard (Original PI)[1], *D. R. Webster (GTRC PI), Feifei Pan*[2]

School of Civil and Environmental Engineering
Georgia Institute of Technology
Atlanta, GA 30332-0355

P. R. Houser, P. E. O'Neill, Ann Hsu[3] *and Yihua Wu*
NASA/GSFC
Hydrological Sciences Branch

September 27, 2002

[1] Currently at: Hydrological Sciences Branch, NASA-GSFC Code 974, Greenbelt, Maryland 20771, Office:301/614-5811 Fax:301/614-5808, E-mail: cpeters@hsb.gsfc.nasa.gov
[2] Currently at: Environmental Sciences Division, Bldg. 1509, MS 6335, Oak Ridge National Laboratory, P.O.Box 2008, Oak Ridge, Tennessee 37831-6335, Phone: (865) 574-9216, e-mail: panf@ornl.gov
[3] Currently at: USDA ARS Hydrology Lab, 104 Bldg 007 BARC-West, Beltsville, MD 20705

Table of Contents

List of Figures

List of Tables

1. Introduction

Accurate assessment of the spatial and temporal variation of soil moisture is essential for addressing many questions on land-atmospheric interaction. Soil moisture is a basic link between the water and energy budgets of land surfaces through its regulation of the partitioning of latent and sensible heat fluxes, its proportioning of rainfall into infiltration and runoff, and its primary control on vegetation development via photosynthesis. Attempts to routinely estimate soil moisture over regional areas using only one source of information (point measurements, remote sensing, or modeling) have been relatively unsuccessful. Recent work has shown that remote sensing combined with water and energy balance modeling in a four-dimensional data assimilation (4DDA) framework provides superior estimates of distributed soil moisture [Houser, 1996]. Although the 4DDA approach has the potential to advect information both horizontally and vertically into data sparse regions, there are significant differences (e.g. measurement depth & area, observation and modeling error, and the definition of soil moisture) between the model predictions and remotely-sensed observations of soil moisture that must be fully characterized to allow their successful integration.

2. Research Objectives

The primary objective of this project is to assess, understand, and predict the relationship between remotely-sensed and modeled soil moisture. This characterization is a necessary prerequisite to successfully integrating remotely-sensed soil moisture observations with models of the land surface water and energy balance, including Soil-Vegetation-Atmosphere Transfer Schemes (SVATS). Soil moisture state variables in SVATS are physically different from remotely-sensed observations of soil moisture due to the nature of both models and observations. SVATS have intrinsic limitations in their agreement with observations because they use simplified or abstract concepts to approximate reality, and their parameters are often empirically based. Microwave remotely-sensed soil moisture observations are strongly affected by surface vegetation, roughness, and temperature variations, and have a dynamic measurement volume. Previous studies have shown that there is a correlation between soil moisture observations and model states, but the physical basis of this correlation is not well understood, and may differ by

climate, season, and model structure. The error covariance between remotely-sensed and modeled soil moisture must be quantified in order to apply 4DDA techniques more rigorous than simple nudging. Characterizing this error structure with respect to other measurable quantities would represent the removal of a significant barrier to the use of remotely-sensed soil moisture in models for water resources management, numerical weather and climate prediction and agricultural production.

This project is assessing, and attempting to understand and predict, the relationship between remotely-sensed and modeled soil moisture through a rigorous inter-comparison of soil moisture predictions made by several fundamentally different SVATS models and remotely-sensed passive microwave soil moisture observations at several different scale, climate, and seasonal regimes. The original research design is given in Table 1 below. Based on the findings land surface intercomparison projects such as PILPS and LDAS, it was decided that the original design would lead to unexplainable differences in soil moisture due to the inherent differences between the various models, while the intent was to explore the degree of model complexity required to represent the spatial pattern of soil moisture. Therefore, the research design was modified as shown in Table 2 to represent a hierarchical modification of a single model (NOAH) to represent vegetation, soils and topographic heterogeneity in the manner of the original models.

Table 1. Summary of the original research design.

Experiment	Data Analysis	Model		
		NOAH	MOSAIC	TOPLATS
MONSOON90	X			
WASHITA92	X			
SGP97	X	X		

Table 2. Summary of the revised research design.

Model/Experiment	Data Analysis	Model		
		NOAH	NOAH+MOSAIC	NOAH+TOPLATS
MONSOON90	X			
WASHITA92	X			
SGP97	X	X		

The originally chosen SVATS models represent a hierarchy of complexity in the representation of spatial heterogeneity, and are the NOAH [Mahrt and Pan, 1984; Chen et al., 1996; 1997], MOSAIC [Koster and Suarez, 1996], and TOPLATS [Famiglietti and Wood, 1994]. The NOAH model is used in the operational NCEP mesoscale forecast and represents a single vegetation and soil class per grid. The MOSAIC model represents vegetation heterogeneity using patches or "mosaics" of vegetation types. The TOPLATS model includes vegetation, topography and soils heterogeneity.

As shown in Tables 1 and 2, these models are being used to make soil moisture predictions at spatial resolutions compatible with microwave soil moisture remote-sensing observations available from three sites: 1) the Walnut Gulch Watershed in Arizona [Schmugge et al., 1994]; 2) the Little Washita Watershed in Oklahoma [Jackson and Le Vine, 1995]; and 3) the Southern Great Plains 1997 Experiment [Jackson, 1996]. The relationships between modeled and observed soil moisture at different scales and climates using different SVATS have been examined using summary statistics, correlation analysis, spatial covariance modeling, and SVATS structural analysis to understand mechanisms that may aid in the prediction of these relationships. It is expected that the proposed strategies will contribute to NASA's Earth Science Enterprise (ESE) science goals by improving our understanding and ability to observe and predict soil moisture, by improving modeled land surface dynamics and spatial heterogeneity, and by ameliorating the land surface data assimilation effort.

3. Accomplishments

The accomplishments on the project reflect those at both GTRC and NASA/GSFC through the first two years of funding. The project was initiated in 1999, and in 2001, a one-year no cost extension of the second year funding at Georgia Tech was requested and approved in order to complete GTRC project tasks, and to accommodate Dr. Peters-Lidard's move to NASA/GSFC. The third year of the project has continued at NASA/GSFC.

The scientific accomplishments on the project have focused on the two areas of analyzing the observed (measured) soil moisture spatial and temporal statistics, and modeling soil moisture for the three sites at which measurements are available. The sections below provide further details regarding the relationships between observed and modeled soil moisture.

3.1. Spatial and temporal structures of measured soil moisture

The spatial and temporal structures of remotely-sensed soil moisture were studied through investigating (1) statistical characteristics and frequency distributions of remotely-sensed soil moisture; (2) the spatial correlation structures of soil moisture fields and correlations among soil moisture, rainfall, and topographic characteristics; (3) scaling characteristics of soil moisture; and (4) a simple method for predicting soil moisture distributions from rainfall data based on the linear stochastic partial differential equation suggested by Entekhabi and Rodrigez-Iturbe (1994).

3.1.1 Statistical characteristics of remotely-sensed soil moisture

The remotely-sensed soil moisture data are from three field campaigns, i.e., Monsoon'90, Washita'92, and SGP'97. These sites are shown in Figure 1 and 2. The coverage, duration and RMSE of each remotely-sensed soil moisture dataset are: 45km^2, 10days, 2 %V/V for Monsoon'90, 900km^2, 8days, 10%V/V for Washita'92, and 10,000km^2, 30days, 3%V/V for SGP'97. Due to weather conditions and other mechanical problems, the actual number of daily soil moisture maps during SGP'97 is 16. The large area coverage and long duration associated with the SGP'97 soil moisture dataset make this dataset particularly unique, because the diversity of soils, vegetation, and atmospheric conditions over SGP'97 domain makes it possible to study the effects of soil, vegetation and atmospheric forcing on soil moisture behavior. In addition, more than one cycle of soil dry-down and wetting was captured during SGP'97, which is also critical for understanding the soil moisture dynamics. Besides remotely-sensed soil moisture, a comprehensive dataset including soil properties (e.g., texture, density, roughness, conductivity), vegetation (e.g., height, LAI, NDVI), gravimetric soil moisture, topography, atmospheric forcing (e.g., wind, radiation, temperature, rainfall) was collected and developed during each field campaign by more than hundreds of participants.

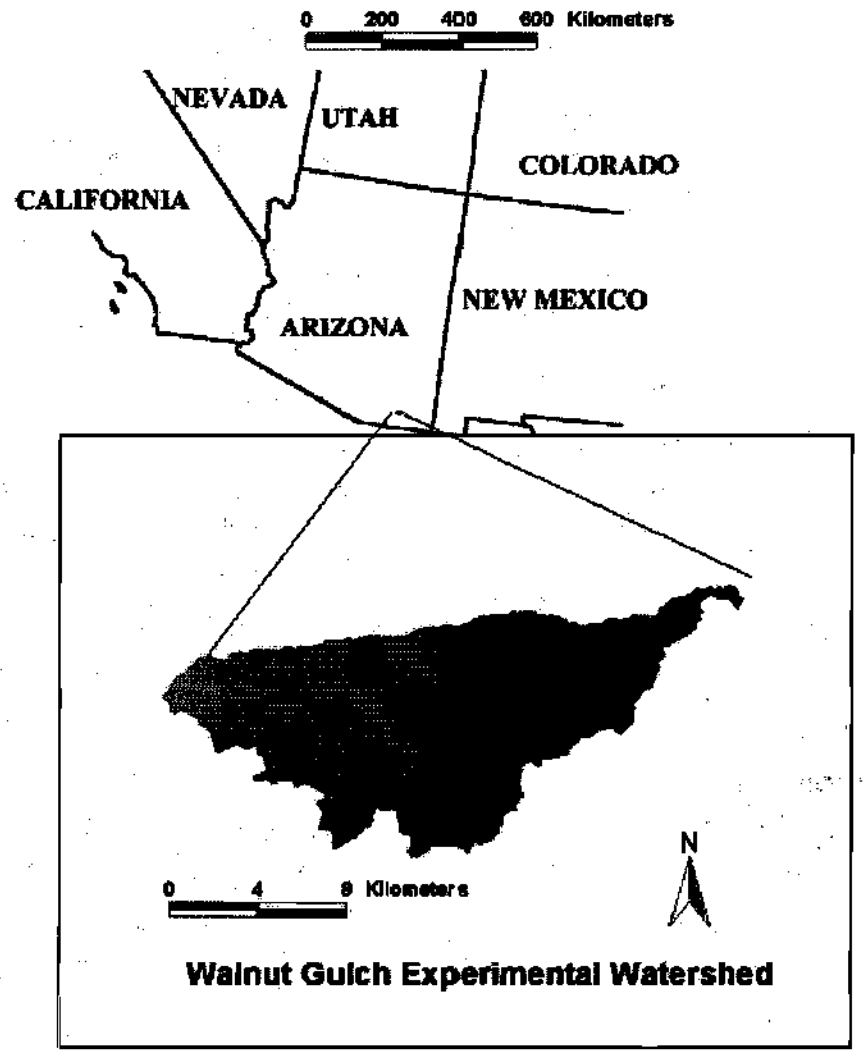

Figure 1. Walnut Gulch Experimental Watershed (WGEW) is in southeastern Arizona.

To describe the distribution of remotely-sensed soil moisture, mean, standard deviation (*sd*), coefficient of variation (*CV=sd/mean*), skewness (γ), and kurtosis (κ) of remotely-sensed soil moisture images were computed. To seek the linkage between soil moisture and precipitation, the statistical moments of daily rainfall fields are also computed.

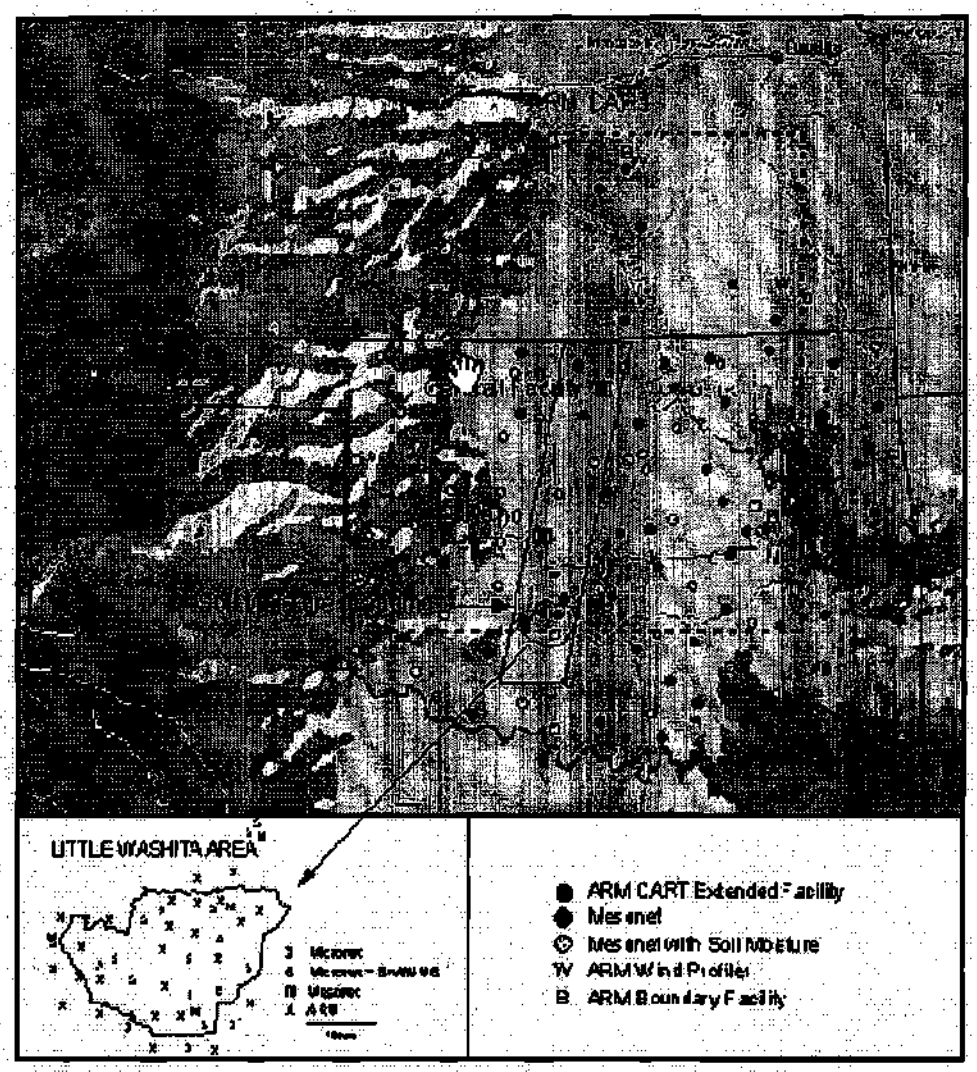

Figure 2. Southern Great Plains Hydrology Experiment area, showing the location of the Little Washita Watershed, Oklahoma.

Time series of mean values and standard deviation for soil moisture and daily rainfall for Monsoon'90, Washita'92 and SGP'97 are given in Figure 3 though 5. These figures indicate that the precipitation plays an important role in controlling soil moisture. However, there is a time lag of soil moisture responding to rainfall, and the effects of rainfall on soil moisture decay with time. The difference in the higher order moments between rainfall and soil moisture fields is also high, especially during SGP'97.

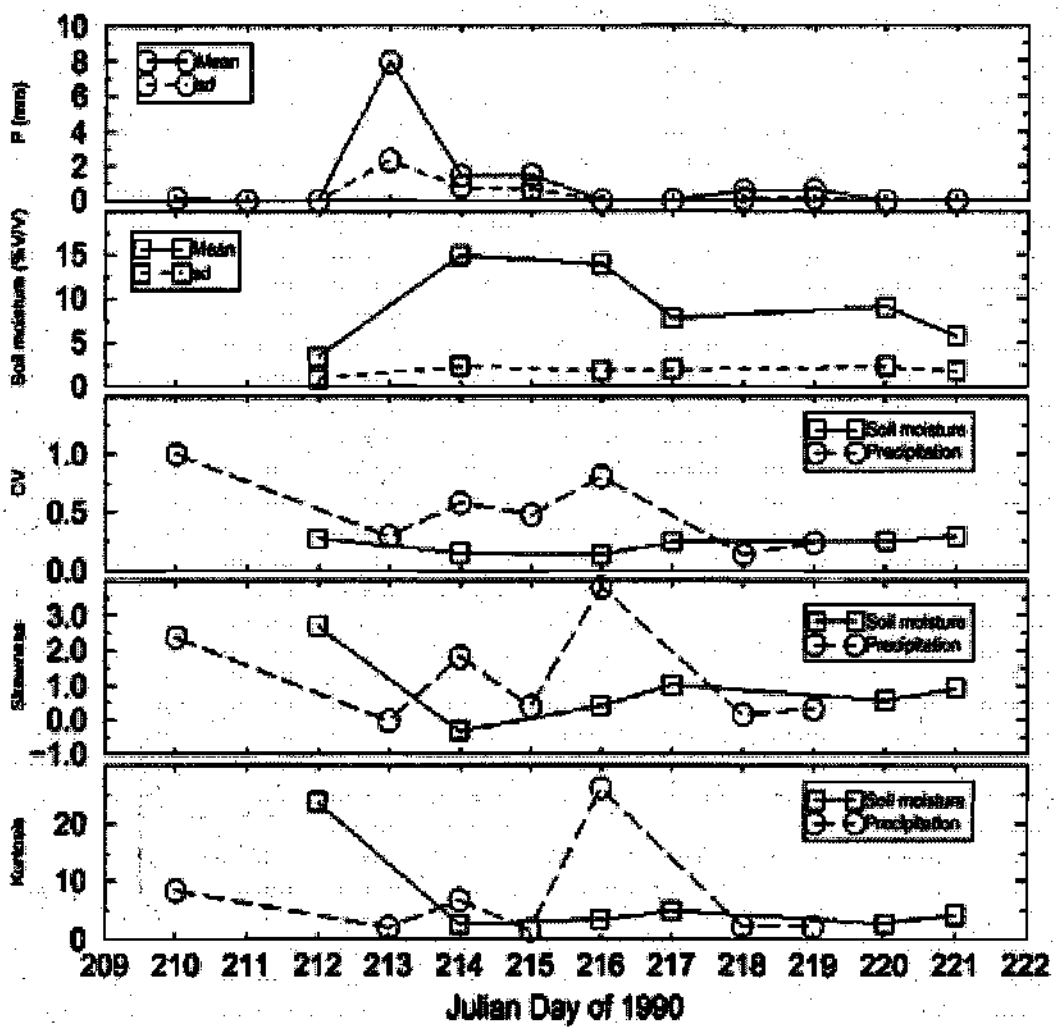

Figure 3. Time series of statistical moments of PBMR derived surface soil moisture and cumulative rainfall during Monsoon'90.

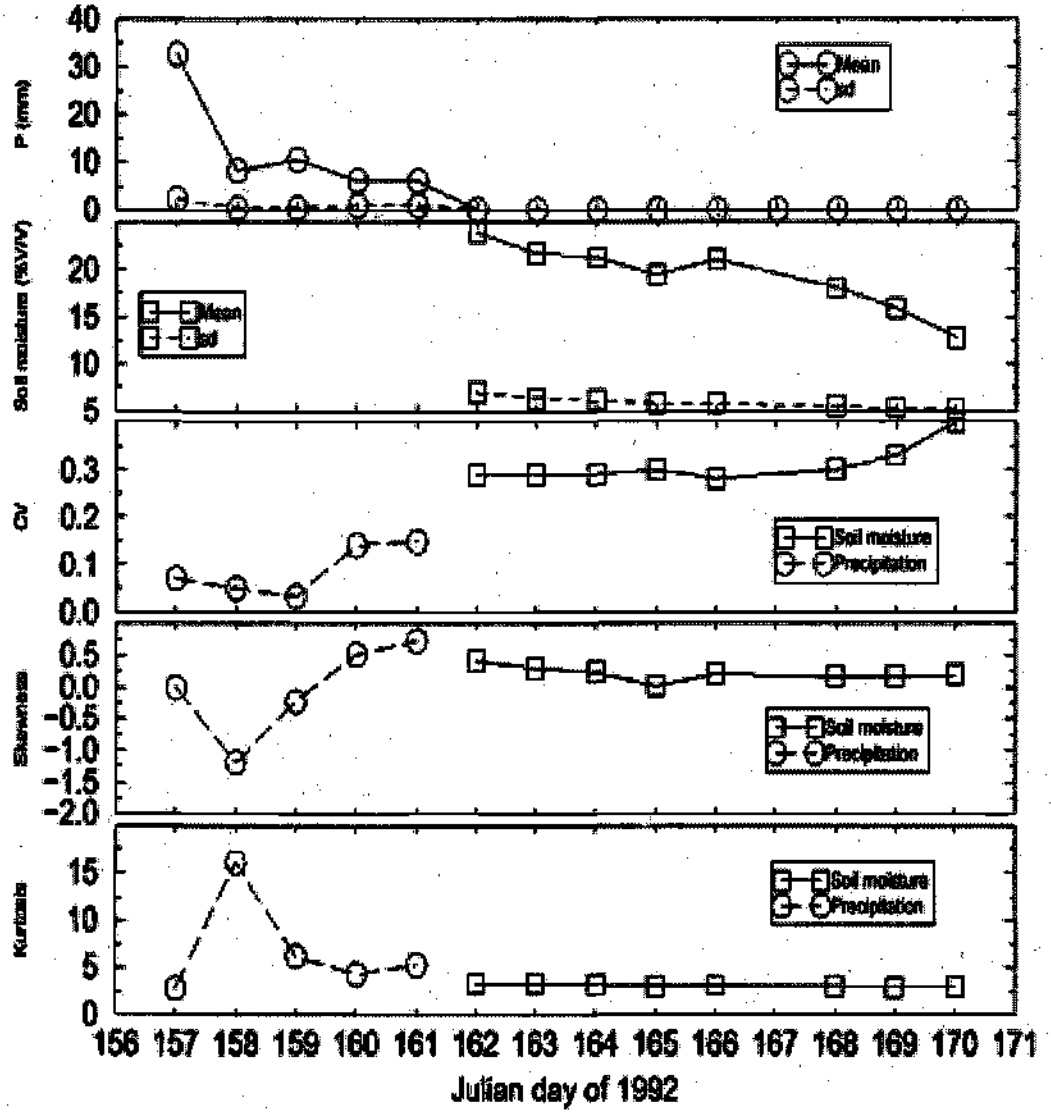

Figure 4. Time series of statistical moments of ESTAR derived surface soil moisture and rainfall fields during Washita'92.

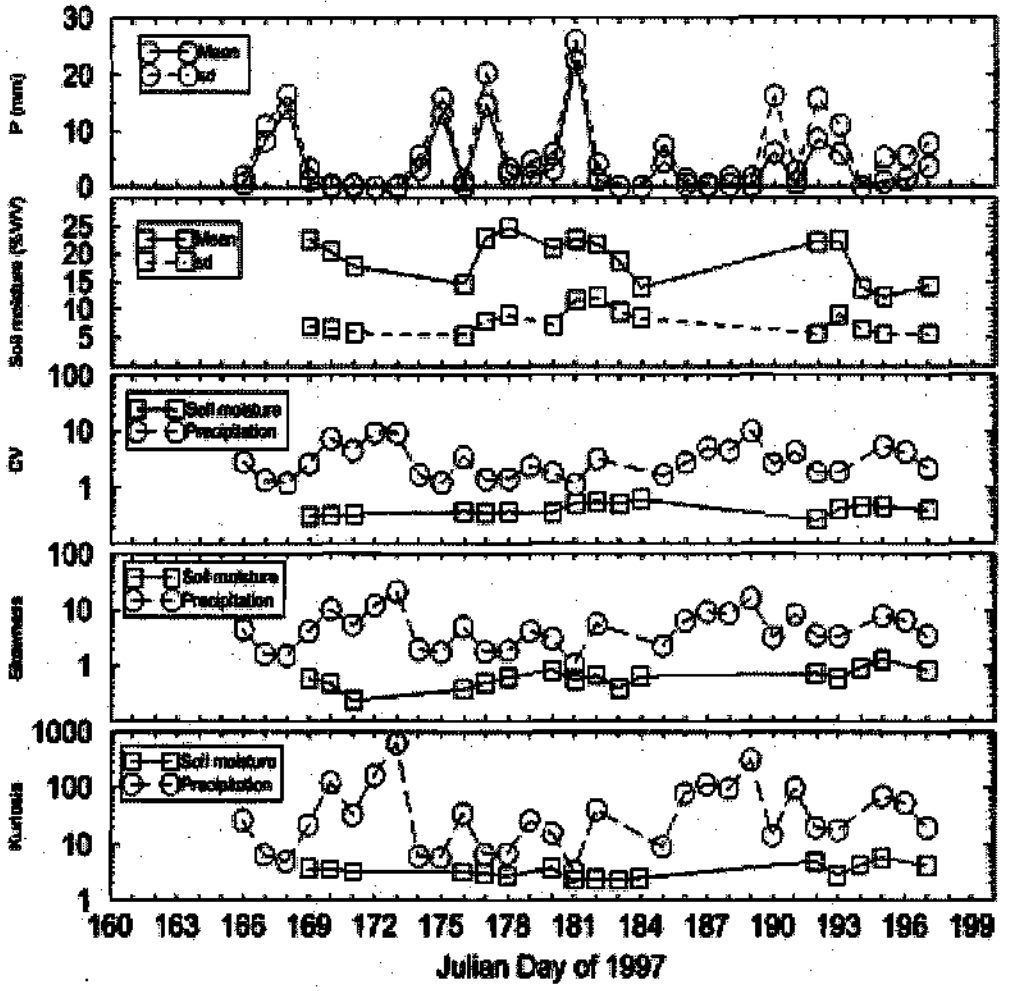

Figure 5. Time series of statistical moments of ESTAR derived surface soil moisture and accumulative rainfall fields during SGP'97.

The scatter plots of mean versus higher order moments of remotely-sensed soil moisture illustrated in Figures 6, 7, and 8 for Monsoon'90--WGEW, Washita'92--LWW, and SGP'97, respectively, show that the scatter plots of mean versus standard deviation and coefficient of variation of remotely-sensed soil moisture images during Monsoon'90 and Washita'92 generally follow those of the ideal soil moisture maps, i.e., standard deviation or variance increases as mean soil moisture decreases while mean versus standard deviation of ESTAR derived soil moisture during SGP'97 departs from that of ideal soil moisture map significantly.

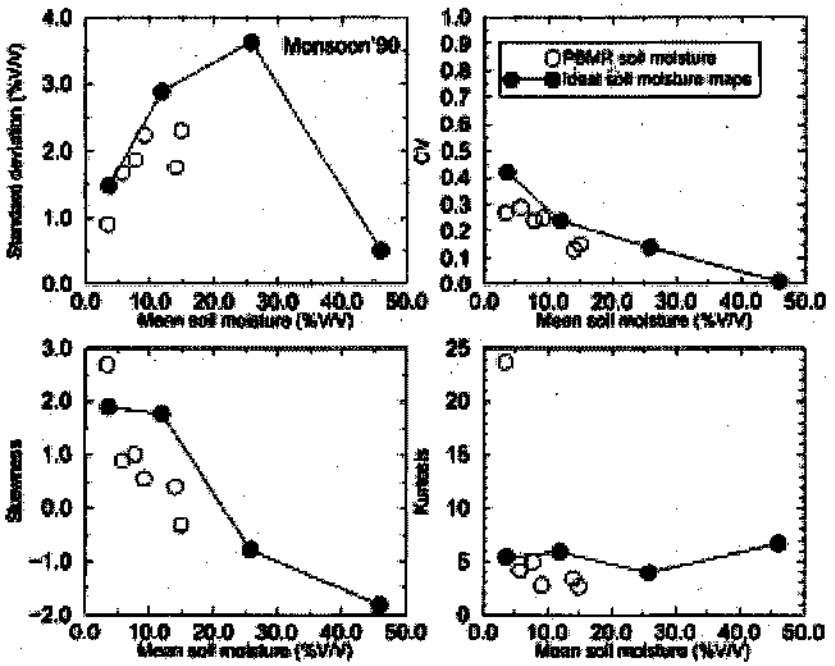

Figure 6. Scatter plots of mean versus standard deviation, CV, skewness, and kurtosis of PBMR derived soil moisture images and ideal soil moisture maps during Monsoon'90.

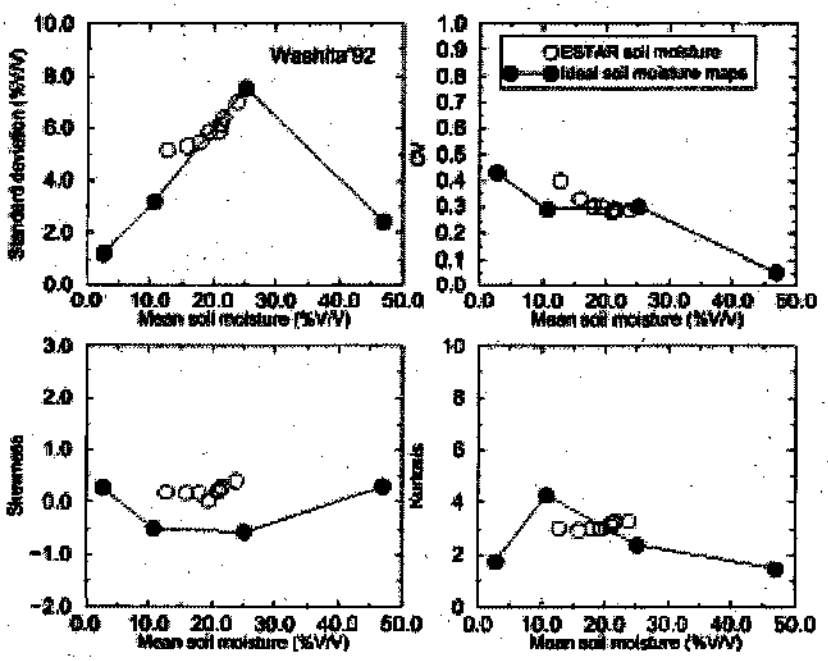

Figure 7. Scatter plots of mean versus standard deviation, CV, skewness, and kurtosis of ESTAR derived soil moisture images and ideal soil moisture maps during Washita'92.

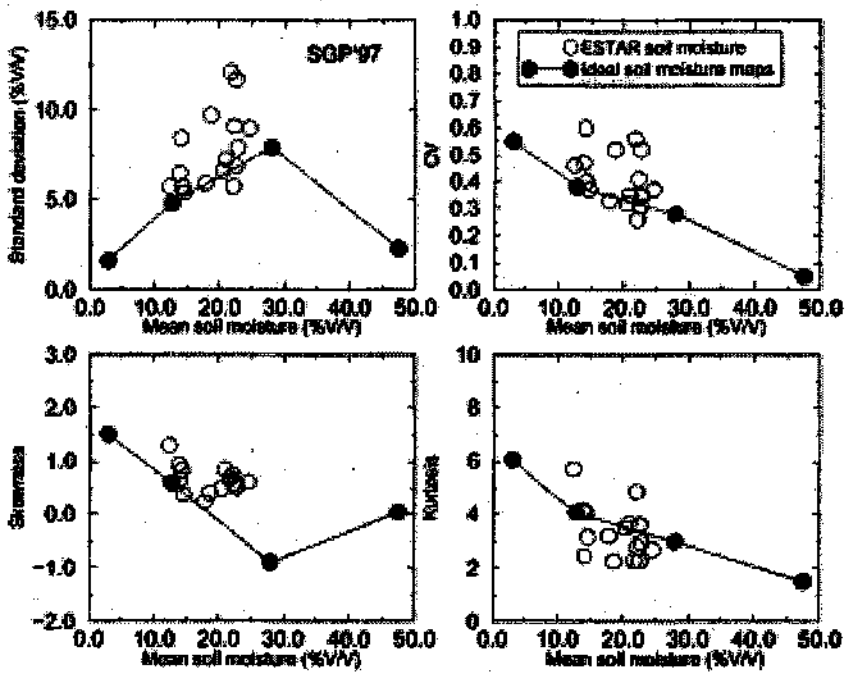

Figure 8. Scatter plots of mean versus standard deviation, CV, skewness, and kurtosis of ESTAR derived soil moisture images and ideal soil moisture maps during SGP'97.

Based on the definition of soil porosity, field capacity, wilting point and residual soil moisture content, soil moisture dynamic range can be divided into three stages: porosity to field capacity, field capacity to wilting point, and wilting point to residual soil moisture. The dry-down process and the associated physics are different during each stage.

When soil moisture is between porosity and field capacity, there is no water limit for evapotranspiration, the dry-down rate due to evapotranspiration is only controlled by the atmospheric conditions, which are relative spatially uniform. Therefore, evapotranspiration can reduce mean soil moisture, but cannot change the spatial variability of soil moisture fields. The other dry-down factor, drainage, is close to the saturated hydraulic conductivity. The negative correlation between porosity and saturated hydraulic conductivity is found among 11 soil textures in Rawls et al. (1982) (i.e., -0.26), and Clapp et al. (1978) (i.e., -0.73). This negative correlation indicates that drainage could increase the variance or standard deviation of soil moisture fields. Therefore, the variance or standard deviation of soil moisture increases with mean soil moisture during the dry-down process. This argument must be verified with observations, since none of the remotely-sensed soil moisture data collected during Monsoon'90, Washita'92, and SGP'97 is in the range of porosity to field capacity.

When soil moisture is between field capacity and wilting point, evapotranspiration is no longer controlled by the atmospheric conditions only, but also by soil moisture condition. The dry-down factor due to evapotranspiration will not only reduce mean soil moisture, but also the standard deviation or variance of soil moisture fields. On the other hand, drainage is no longer close to the saturated hydraulic conductivity. The positive correlation between soil moisture and hydraulic conductivity (Feifei Pan, 2002) indicates that the spatial variability of soil moisture fields will be also reduced by drainage. Overall, variance or standard deviation of soil moisture fields decreases as mean soil moisture decreases, if mean soil moisture is between field capacity and wilting point. This behavior is shown in the remotely-sensed soil moisture fields (see Figures 6, 7 and 8).

When soil moisture is between wilting point and residual soil moisture, evapotranspiration is close to zero. Drainage is the only dry-down factor, which is still positively correlated with soil moisture. Therefore, the standard deviation or variance of soil moisture fields will also decreases with dry-down process, if mean soil moisture is in the range of wilting point to residual soil moisture. This behavior is shown in PBMR derived soil moisture fields during Monsoon'90 (see Figure 7).

3.1.2. Spatial Correlation Structures of Soil Moisture Fields

To understand the effects of rainfall on soil moisture spatial structures, the covariance function of moving average and weighted average rainfall maps during Monsoon'90, Washita'92, and SGP'97 were calculated, and the correlation length of each rainfall field is estimated from the plot of covariance coefficient versus lag distance. Figures 9, 10 and 11 show the time series of correlation length of remotely-sensed soil moisture and the correlation length of rainfall for Monsoon'90, Washita'92, and SGP'97, respectively. It is shown in these figures that shortly after or during rainfall events, the correlation length of soil moisture is dominated by precipitation. After rainfall events, the correlation length of soil moisture field decays during the dry-down process, and finally approaches spatial correlation structures of land surface characteristics. This behavior is consistent with the results shown in the previous section, i.e., soil moisture is strongly

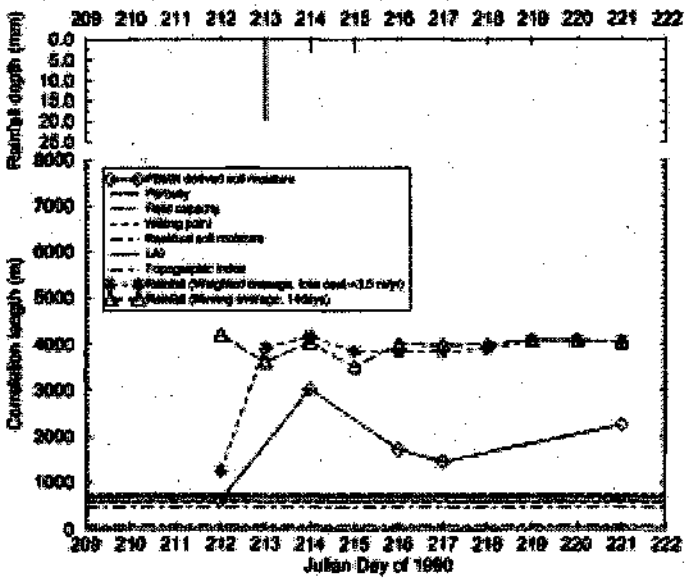

Figure 9. Time series of daily rainfall depth, correlation lengths of remotely-sensed soil moisture, moving average and weighted rainfall during Monsoon'90. The correlation lengths of porosity, field capacity, wilting point, residual soil moisture, LAI, and topographic index are labeled.

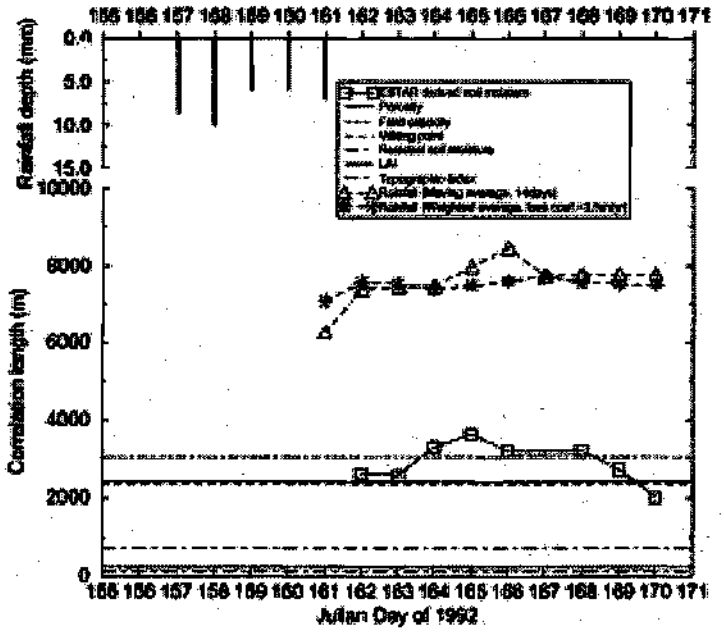

Figure 10. Time series of daily rainfall depth, correlation lengths of remotely-sensed soil moisture, moving average and weighted rainfall during Washita'92. The correlation lengths of porosity, field capacity, wilting point, residual soil moisture, LAI, and topographic index are labeled.

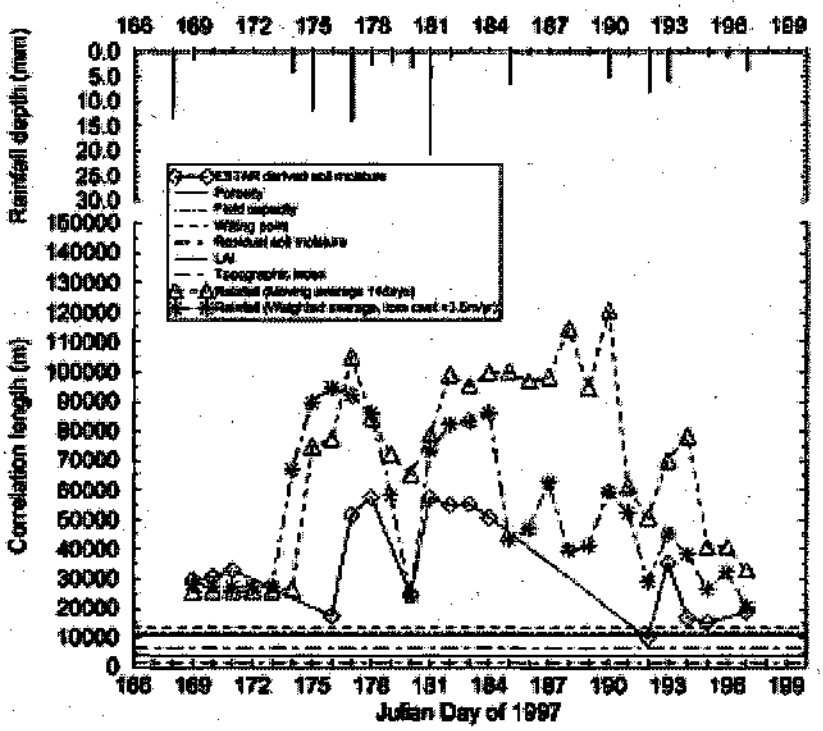

Figure 11. Time series of daily rainfall depth, correlation lengths of remotely-sensed soil moisture, moving average and weighted rainfall during SGP'97. The correlation lengths of porosity, field capacity, wilting point, residual soil moisture, LAI, and topographic index are labeled.

correlated with rainfall during and shortly after rainfall events. During the dry down period, the land surface characteristics, i.e., soil and land cover, play an important role in controlling soil moisture spatial structures, and the influences of rainfall on soil moisture are reduced by the dry down process (i.e. drainage, evapotranspiration and surface runoff).

3.1.3. Scaling Characteristics of Soil Moisture

Analysis of the scaling characteristics of the remotely-sensed soil moisture fields for Monsoon'90, Washita'92 and SGP'97 has led to the identification of three regimes during the dry-down process: atmosphere—dominated (Regime 1), transitional (Regime 2), and land surface characteristics—dominated (Regime 3). The multi-scaling characteristics are reduced in Regime 1, and intensified in Regimes 2 and 3. The intensification rate in Regime 2 is less than that in Regime 3 (as shown in Figures 12, and 13). The same multi-scaling behavior of Washita'92 soil moisture fields has been shown in Peters-Lidard et al. (2001), which is different

from previous work by Rodriguez-Iturbe et al. (1995) and Hu et al. (1998). They all showed that the multi-scaling characteristics of soil moisture are intensified monotonically during the dry-down period. One possible reason is that Rodriguez-Iturbe et al. (1995) only pick three soil moisture maps with a 2- or 3-day gap for scaling analysis.

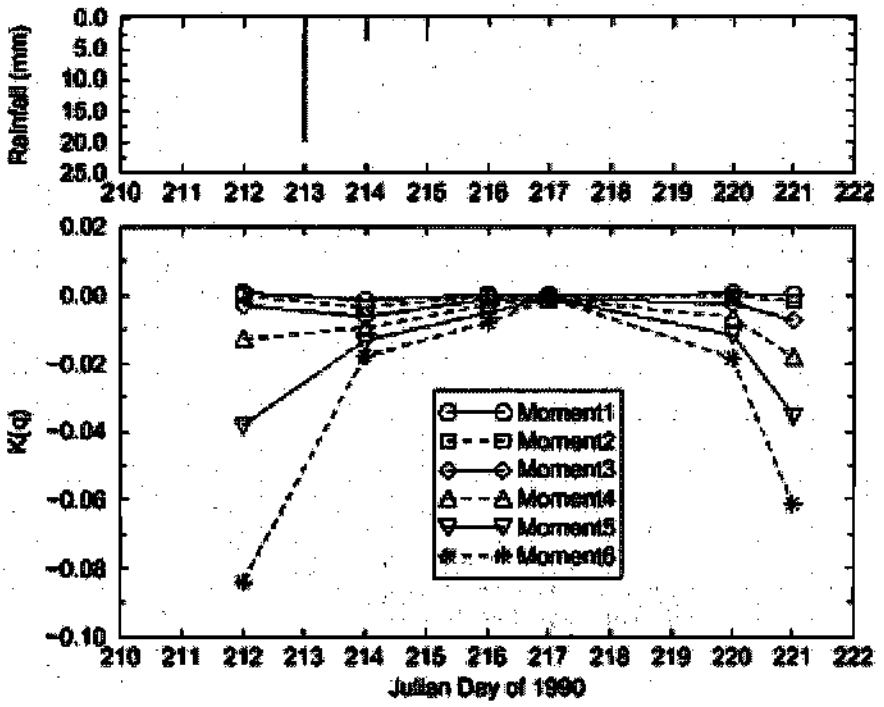

Figure 12. Time series of scaling exponents of PBMR derived soil moisture during Monsoon'90.

Although the three stages were suggested as early as in early 1950s, the transition from one stage to another stage is difficult to determine only based on the soil moisture measurements (Jackson, 1973). This may be the reason why the concept of three stages of soil drying is seldom mentioned or used after the concept was suggested. Now with access to remotely-sensed soil moisture data, we can identify those three regimes from the time series of scaling exponent, and thus advance our understanding of the drying process occurring in soil.

3.1.4. Stochastic Soil Moisture Model

To gain insight into the physical controls on soil moisture spatio-temporal structures, a stochastic model linking precipitation fields to soil moisture fields is developed. The derivation of the model shows that information on the time-weighted ratio of the rainfall rate to the loss

coefficient is required to represent the transition between atmospheric-dominated and land surface characteristic-dominated states. Although this model consists of a simplified representation of soil moisture dynamics, it represents the two key processes identified previously, i.e., dry-down and wetting. The dry-down process is controlled by evapotranspiration and drainage, which is lumped into one loss term, and the wetting process is controlled by precipitation and diffusion. Through studying the topographic effects on soil moisture, which are due to diffusion, we find that the dominant wetting factor for the cases studied is precipitation, not diffusion. Moreover, it is also found that the topographic effects of soil moisture could be misinterpreted if the correlation between precipitation and topography is not considered. This finding explains why there exists a contradiction related to the topographic effects on soil moisture fields, as discussed in Famiglietti et al. (1998).

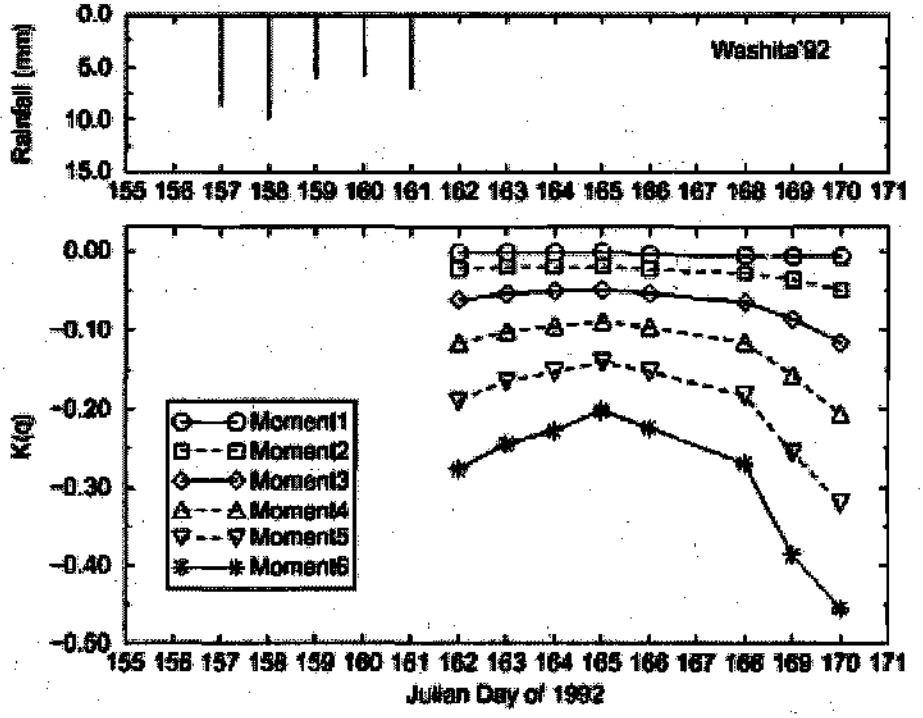

Figure 13. Time series of scaling exponents of ESTAR derived soil moisture during Washita'92.

The transition from atmosphere to land surface control of soil moisture fields is further explained by two studies in the thesis: analysis of the temporal geostatistics of observed soil moisture and analysis of the loss function in the analytic model. Through studying the correlation lengths of soil moisture, rainfall and land surface characteristic fields, it is found that the

correlation lengths of soil moisture fields are increased due to precipitation. After the storm events stop, the correlation lengths of soil moisture fields decay and approach those of land surface characteristics, rather than just soil properties as shown in Yoo et al. (1998). One reason is that vegetation and its related evapotranspiration are not included in their study.

Analysis of the loss coefficients estimated using the observed soil moisture (Figure 3.25) indicates that the simple analytic model developed in this chapter can represent the dominant physics in the wetting and drying phases. Over the Monsoon'90 and Washita'92 domains, it is found that saturated hydraulic conductivity (K_s) and leaf area index (LAI) serve as surrogates of the physics involved in the dry-down process, i.e., a large loss coefficient is associated with a fast drainage (i.e., large K_s), and a strong transpiration directly from surface soil rather than from vegetation cover (i.e., small LAI). Although in theory the loss coefficient should also depend on the radiative and turbulent transfer processes that control evapotranspiration, in a micro-to-mesoscale watershed (<1000km^2), the vegetation variability dominates the atmospheric variability in the determination of the loss coefficient. However, for different temporal and spatial scales, as well as applications in different climates, it is likely that these effects cannot be ignored.

A small RMSE in the estimated catchment mean soil moisture (i.e., 5 %V/V) and a high correlation coefficient (0.83), as shown in section 3.5.3, indicate that the stochastic model provides us a robust tool to predict soil moisture based on rainfall observations and information of local land surface characteristics, as well as a way to gain physical insight into the soil moisture process. One advantage associated with this method is that no initial condition of soil moisture is required.

3.2. Spatial and temporal structures of modeled soil moisture

3.2.1. The TOPLATS Model

Using the TOPLATS model, we have investigated the spatial structure of surface fluxes and states for the Washita'92 field experiment and the August campaign of the Washita'94 field experiments. For Washita'92, the model is validated against gravimetric (see Fig.1) and remotely-sensed soil moisture (see Fig.2), and for Washita'94, the model is validated against gravimetric soil moisture (see Fig.3) and measured energy fluxes. The model is shown to

reasonably represent land-atmosphere inter-actions during the experimental periods. Scaling analysis of soil moisture and latent heat flux is indicative of multiscaling behavior. The temporal behavior of the scaling exponents for various moments suggests the existence of three distinct regimes during a dry-down. The multiscaling behavior of soil moisture and latent heat flux is hypothesized as a relationship that is a function of average soil moisture, and this relationship seems to fit the data quite well. Similar scaling analysis of important land surface properties indicates simple scaling for porosity, field capacity, and wilting point, and multiscaling for residual soil moisture, leaf area index and the soils-topographic index. This is consistent with model results, which indicate a transition from simple scaling to multiscaling with dry-down. It is hypothesized that this transition is governed by the scaling properties that in wet conditions control infiltration (porosity, field capacity, leaf area index) to properties that in dry conditions control drainage (residual moisture content and soils-topographic index) and evaporation (wilting point, leaf area index). Land surface models that fail to incorporate these features will most likely be unable to capture the dynamic nature of soil moisture spatial variability.

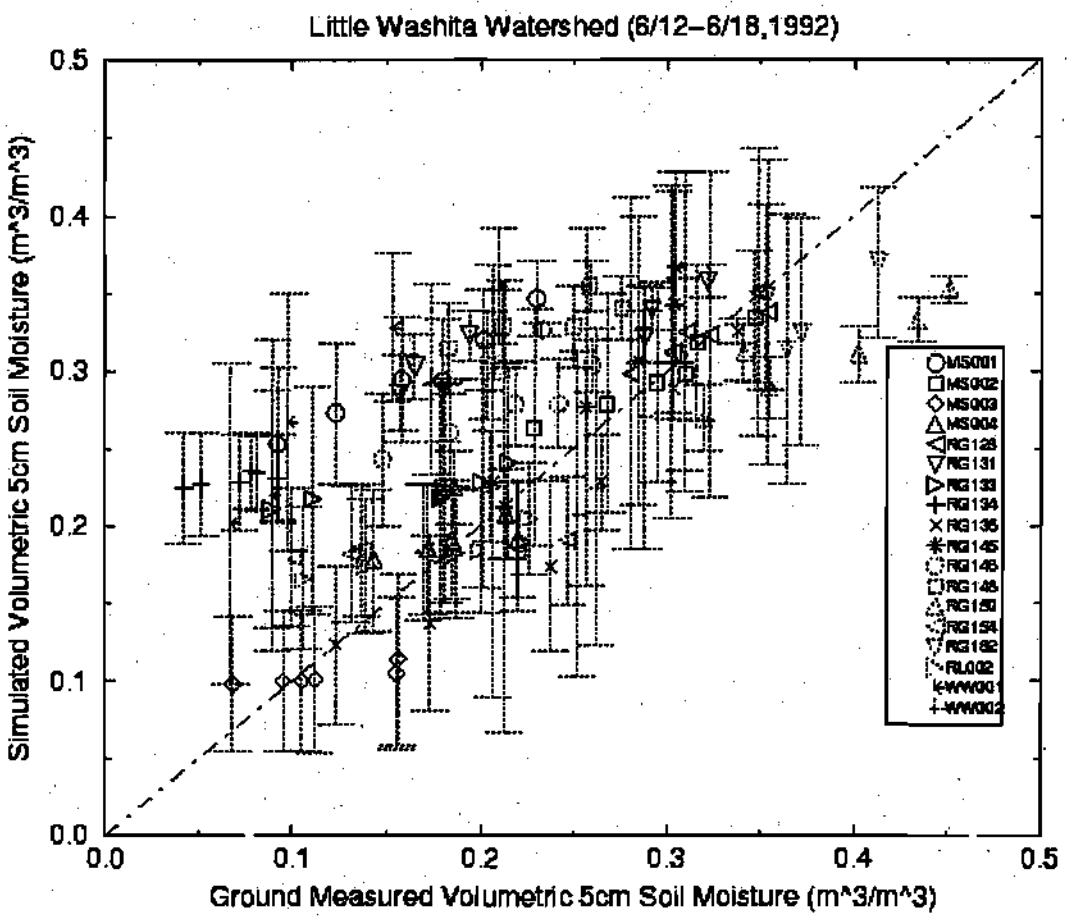

Figure 14. Scatter plot of field-scale gravimetric versus modeled 5 cm soil moisture for period June 12-18, 1992. The error bars represent the standard deviation of the gravimetric measurements for each field.

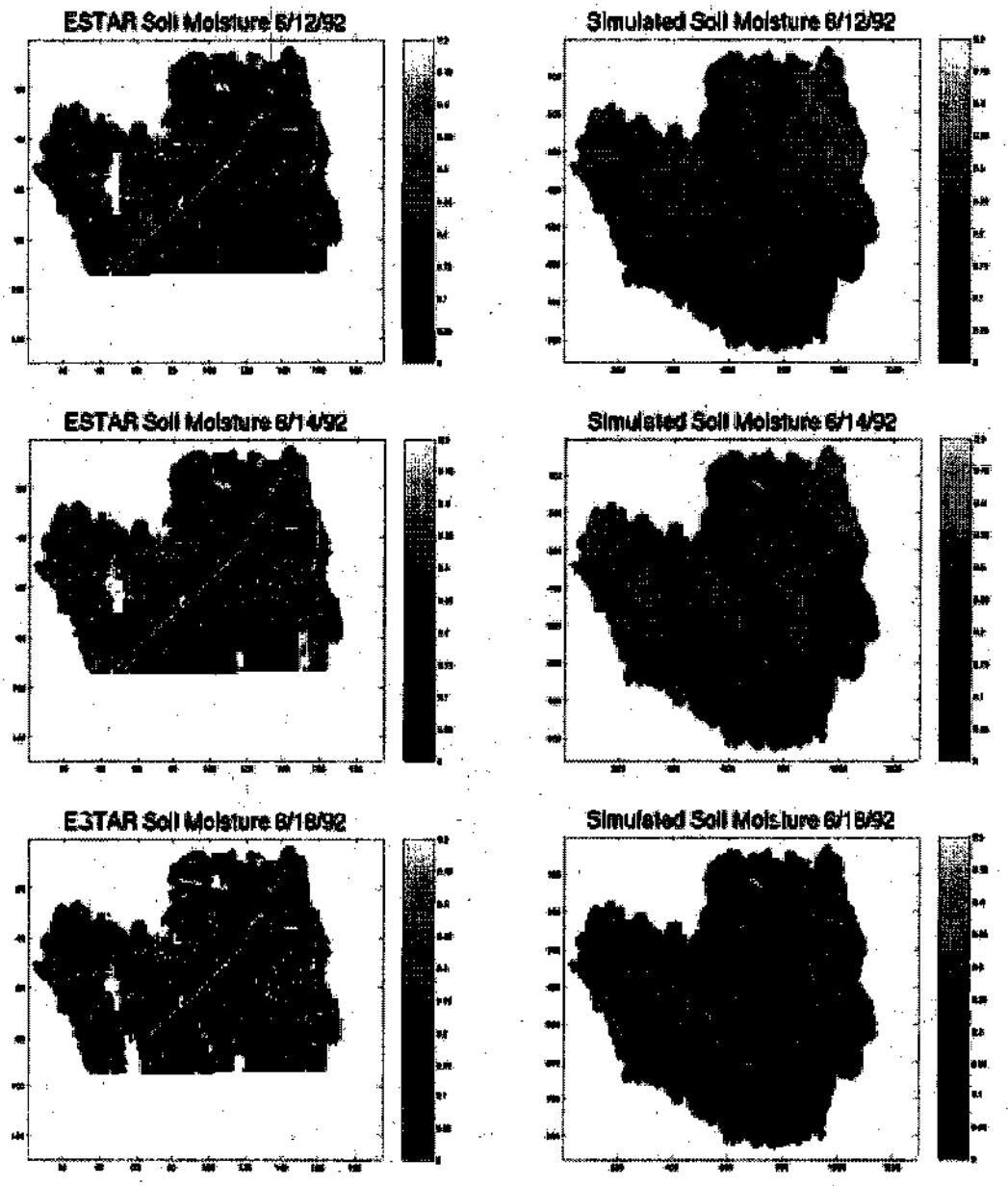

Figure 15. Images of ESTAR and model-derived 5 cm soil moisture for June 12, 14, and 18,1992. ESTAR resolution is 200m, and model resolution is 30m.

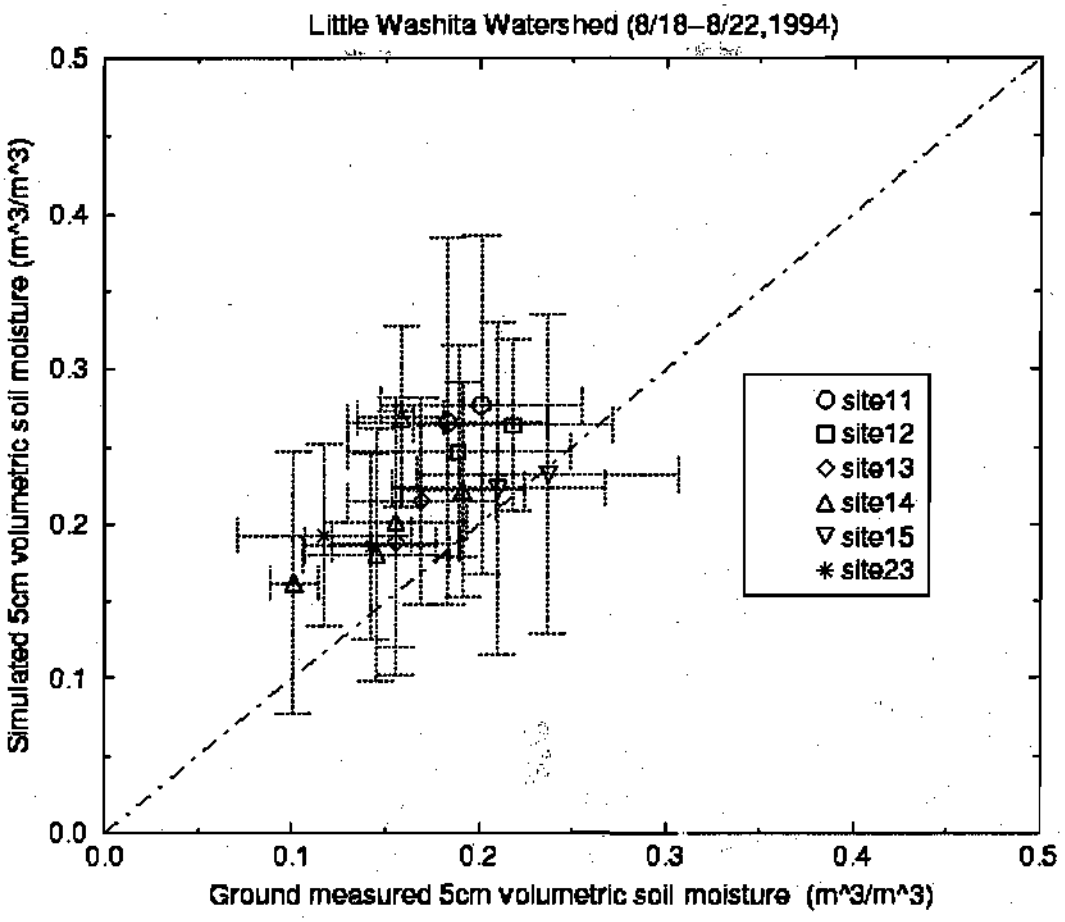

Figure 16. Modeled and gravimetric 5 cm volumetric soil moisture for the August Washita'94 field program. Error bars indicate standard deviations for gravimetric and modeled fields.

3.2.2. The NOAH Model

In order to calibrate and verify the performance of the NOAH model for the SGP97 test region, a one-dimensional version of NOAH was first run at the point scale for the Central Facility grazed pasture field CF01. A variety of ground data exists for CF01, including truck-mounted L and S band microwave radiometer (SLMR) measurements, ARM, flux tower, and tethersonde meteorological and boundary layer data, soil pit measurements, and limited TDR and gravimetrically sampled surface soil moisture data, which facilitate model initialization, implementation, and verification. Average water content of the sparse vegetation in the grazed pasture in CF01 was ~ 0.153 kg/m^2.

In the one-dimensional model run, NOAH was initialized by soil moisture and temperature profiles and driven by seven meteorological forcing parameters from ARM (air temperature, humidity, surface pressure, wind speed, surface downward solar and longwave radiation, and precipitation) for the entire month-long SGP97 experimental period. The resulting model output for predicted soil moisture at 3 cm was then compared to available time series ground measurements of soil moisture. The ground measurements used in this comparison consisted primarily of 3 cm soil moisture from the GHCC soil pit installed next to the SLMR footprint in CF01. However, the pit data were known to have a bias in that they did not accurately reflect wet soil moisture conditions immediately following rainfall events. For this reason, the NOAH model output was also compared to sporadic TDR measurements taken adjacent to the SLMR footprint. A plot of these data is shown in Figure 17.

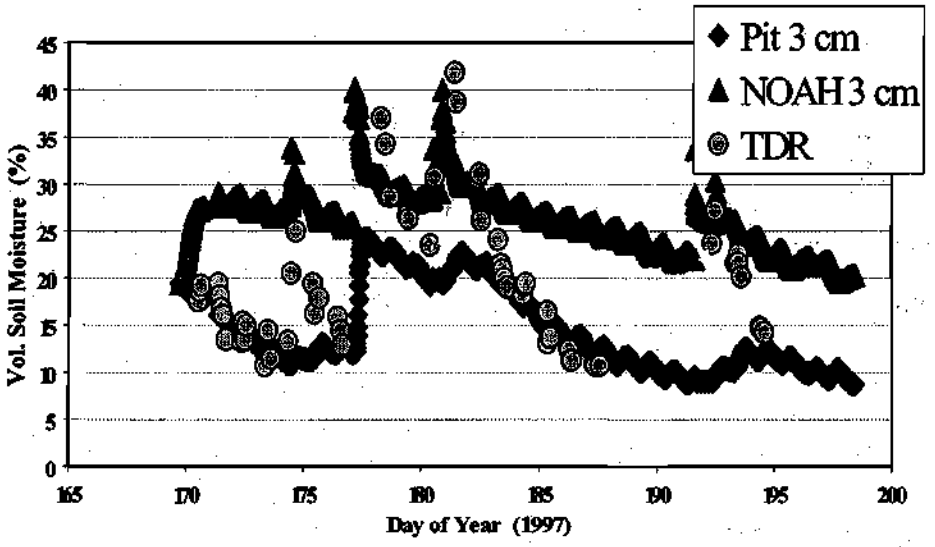

Figure 17. NOAH model results for the Central Facility during SGP97.

As seen in Figure 17, after an initial period of model spin-up and stabilization, the 1-D NOAH model output does a good job of matching the temporal variation in the measured pit soil moisture data throughout the experiment and approximates the high soil moisture values obtained from the TDR sensors after rainfall. However, the model fails to dry out the soil sufficiently to match ground measurements between rainfall events. Parameters that may affect the model soil moisture output include albedo and green vegetation fraction. The values used for these parameters in the 1-D NOAH model are monthly averages over a few years of AVHRR observations provided by NCEP at 1/8 degree resolution, which might not be representative of

the actual SGP97 conditions. When model fluxes were compared to measured flux data, it was determined that the NOAH model also overestimated net radiation and sensible heat all of the time and underestimated latent heat.

Although preliminary assessment of the 1-D NOAH model run indicates general agreement with ground truth measurements, it appears necessary to adjust some of the model input parameters. A locally specific albedo and green vegetation fraction were generated using VISIR data from the TMS sensor during SGP97 and evaluated in terms of improvements in model performance.

In preparation for running the full two-dimensional version of NOAH over the entire 11,000 km^2 SGP97 test region for comparison with the ESTAR-derived soil moisture maps, the randomly distributed MESONET measurements were interpolated to the 800 m ESTAR image grid. The model domain has a size of 349 by 175 grid points covering the entire 11,000 km^2 SGP97 test region. The model was run for comparison with the ESTAR-derived soil moisture maps.

Several 2D runs were conducted using MESONET precipitation and NEXRAD precipitation observations as driving force with different soil moisture initializations and vegetation types: 1. Using MESONET soil moisture profiles to initialize 2D NOAH. 2. Using ESTAR derived soil moisture on June 18 to adjust moisture profile obtained from MESONET measurement and then to initialize the 2D NOAH. 3. Using a merged 0-5 cm soil moisture image to adjust moisture profile and then to initialize the 2D NOAH. 4. Using different vegetation types: a) the entire image is classified as ground cover (ivegtyp=7), b) If more than 35% of an ESTAR pixel was classified as trees in the SGP97 land cover data, this pixel is classified as BROADLEAF-DECIDUOUS TREES in NOAH's scheme (ivegtyp=2).

Several statistical parameters were computed for comparisons between model outputs and observations: mean, rms, bias, absolute and relative differences between predicted hourly soil moisture with precipitation data from MESONET and NEXRAD. Other statistics included the percentage of grid points with relative difference less than certain values, percentages of grid points with negative and positive bias.

Generally speaking, model overestimates soil moisture in all runs with both MESONET and NEXRAD rainfall inputs (Figure 18) except day 169 and 178. As the run time increases, number of grid points with overestimation also increases. Therefore, the bias

and RMS also increase with run time (Figure 19). This suggests that lost terms simulated in the model, such as evapotranspiration and drainage, are not big enough, extra soil water accumulated in the soil. This is also suggested in the comparison between runs with different vegetation types (See discussion in next paragraph).

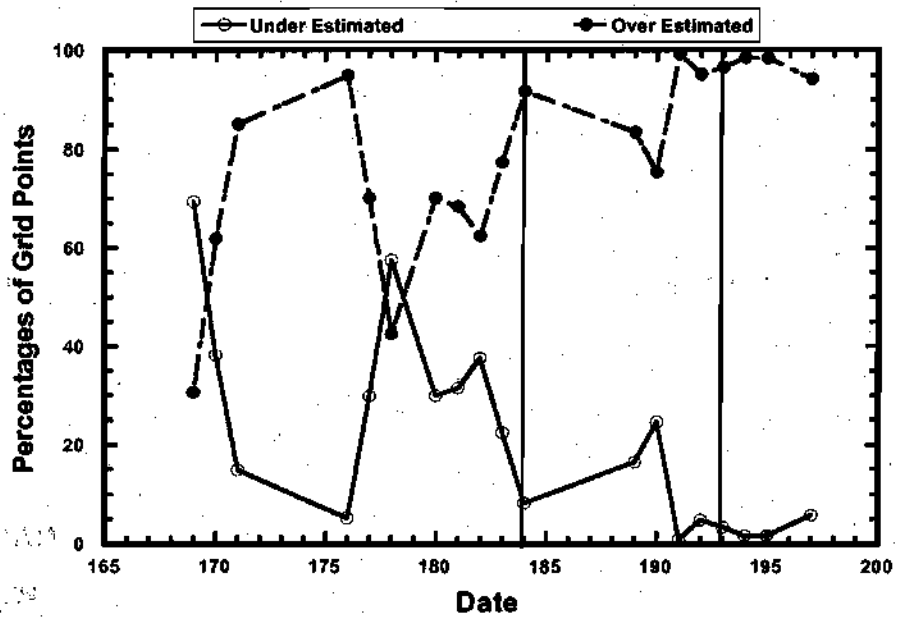

Figure 18. Percentages of grid points of underestimated and overestimated soil moisture.

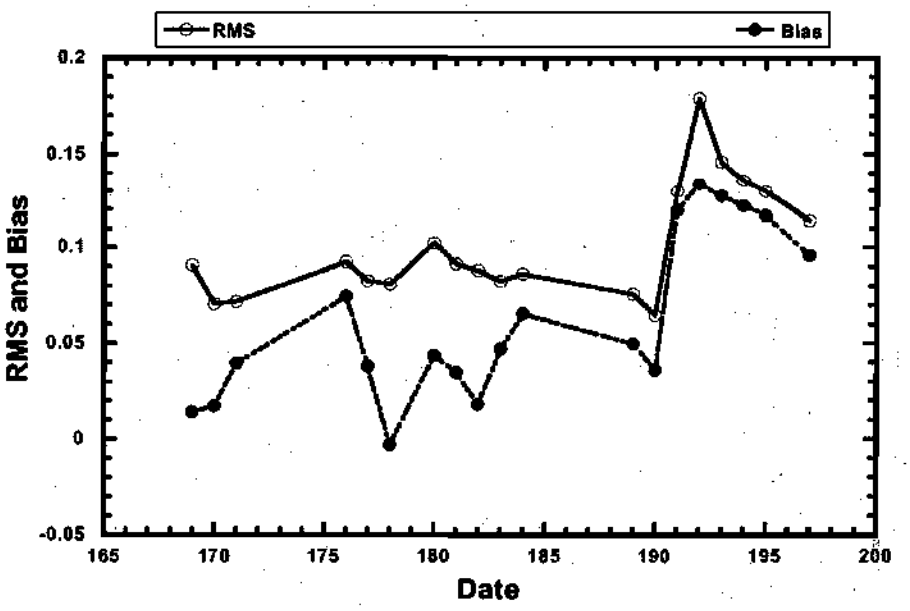

Figure 19. Averaged bias and RMS error for the SGP97 domain.

Accumulation of MESONET and NEXRAD precipitation from June 18 to July 17, 1997 is shown in Figure 20. The major distribution patterns of the accumulated rainfall are very similar: more rainfall at the north end than at the south end of the domain. However, distribution differences between MESONET and NEXRAD observations are very clear. It would be expected that modeled soil moisture difference exits between runs with MESONET and NEXRAD. Figures 21 through 24 show differences between runs with MESONET and NEXRAD precipitation.

Figure 20. Total rainfall observed by MESONET and NEXRAD during the entire SGP97.

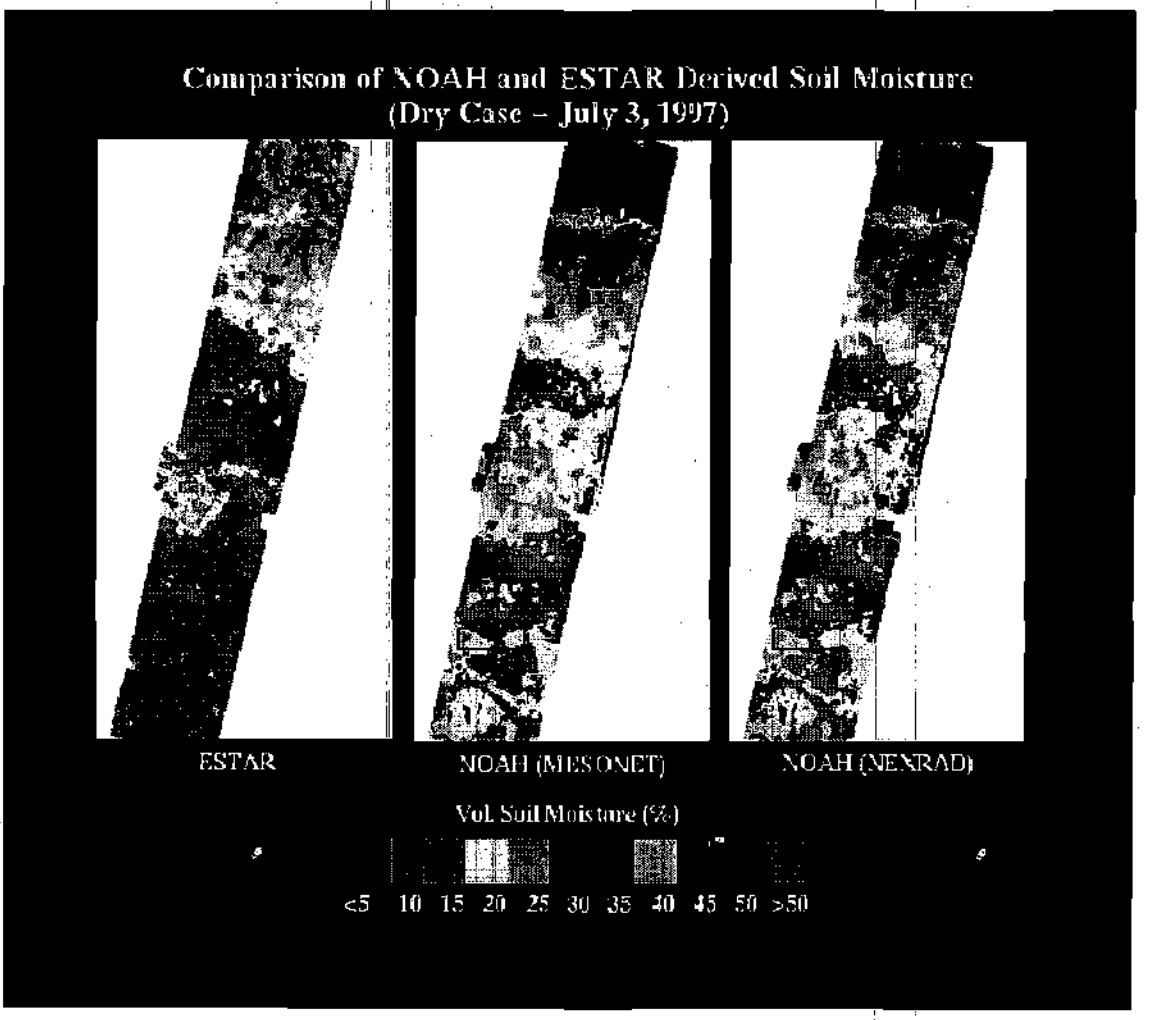

Figure 21. Comparison of model output with ESTAR derived soil moisture on the dry day.

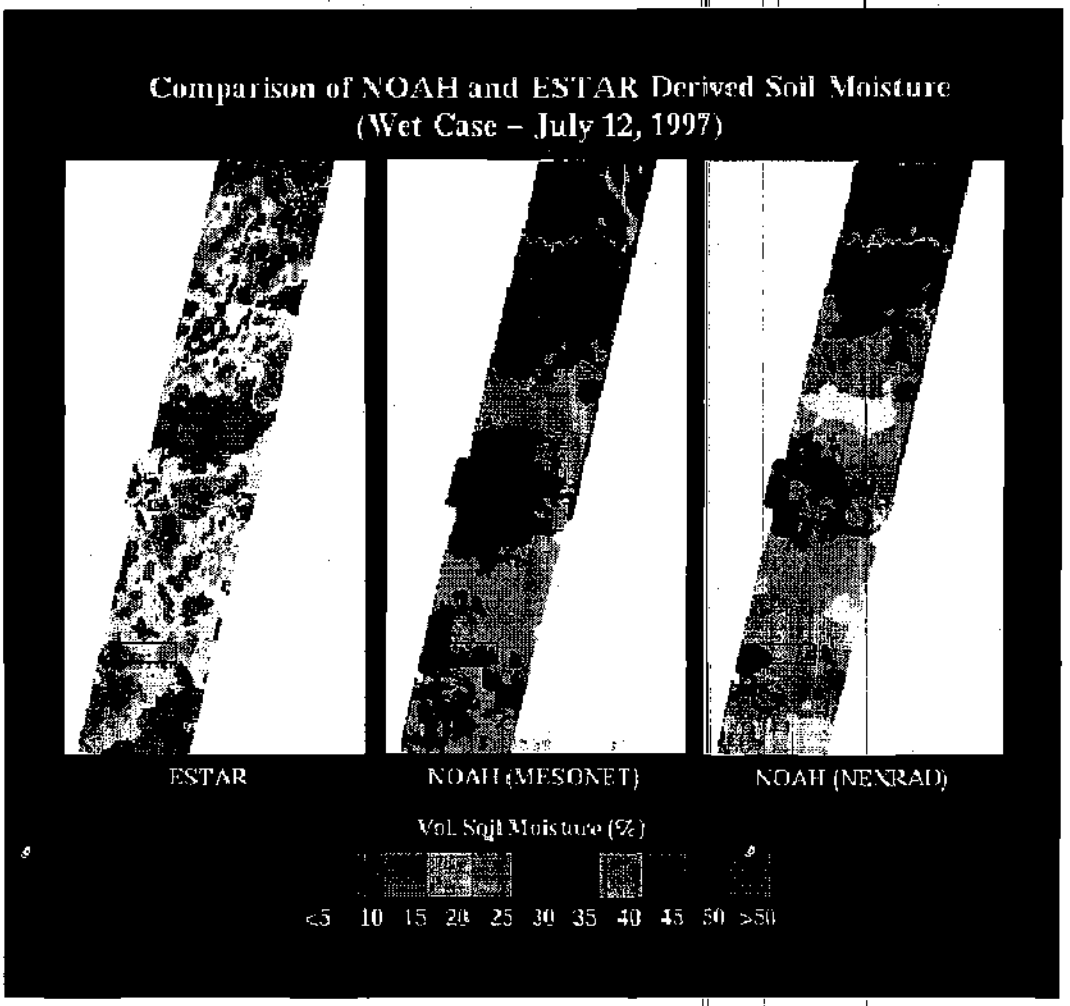

Figure 22. Comparison of model output with ESTAR derived soil moisture on the wet day.

Comparisons between Figure 22 and 23 show that vegetation plays a very important role in soil moisture simulations. Model output in Figure 22 reflects the vegetation type for the entire domain classified as ground cover, (ivegtyp=7), while model output in Figure 23 reflects a refined approach in which if more than 35% of a ESTAR pixel was classified as trees in the SGP97 land cover data, the pixel is classified as BROADLEAF-DECIDUOUS TREES in NOAH's scheme (ivegtyp=2). The run with both vegetation types is clearly better the run with only ground cover.

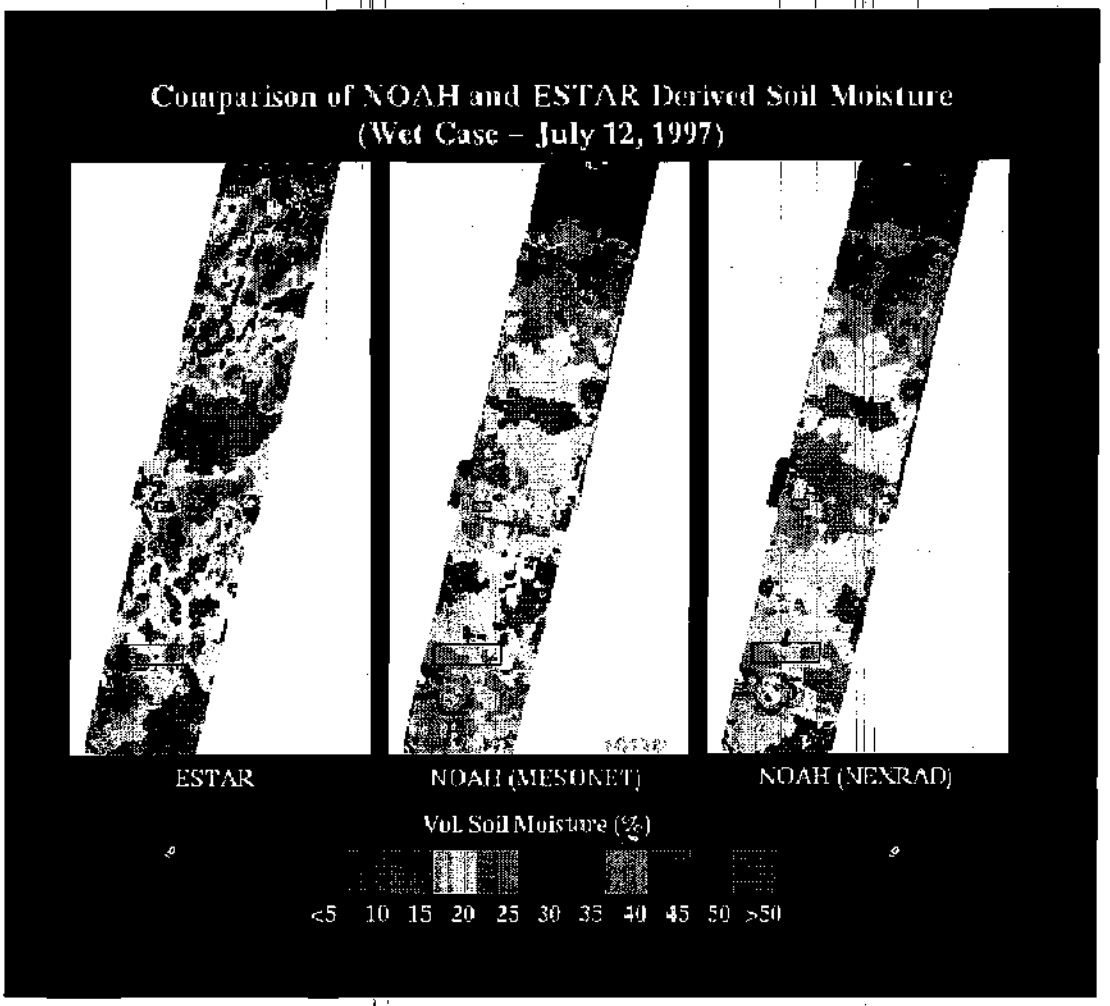

Figure 23. Comparison of model output with ESTAR derived soil moisture on the wet day. Vegetation for this run is set to a mix of ground cover and broadleaf deciduous trees.

4. Future Work

Future project plans will focus on the following issues:

- **Modify the driver program for NOAH model**
- **Run the NOAH model over MONSOON90 and Washita92 experiments.**
- **Run the NOAH model with features of MOSAIC and TOPLATS over MONSOON90, WASHITA92 and SGP97**
- **Further validating modeled soil moisture against observations and investigate vegetation type effects.**

5. Publications and Presentations

5.1. Publications

Peters-Lidard, C. D., F. Pan, and E. F. Wood, 2001. A re-examination of modeled and measured soil moisture spatial variability and its implications for land surface modeling. *Advances in Water Resources*, Vol 24/9-10, pp 1069-1083.

Pan F., and C.D. Peters-Lidard, 2001: Downscaling and assimilating remotely-sensed soil moisture data for the TOPLATS model. Abstract submitted to American Geophysical Union 2001 Spring Meeting.

Pan F., 2002: Spatial and Temporal Structures of Soil Moisture Fields, Ph. D Thesis, School of Civil and Environmental Engineering, Georgia Institute of Technology.

5.2. Presentations

Peters-Lidard, C. D., P. E. O'Neill, A. Hsu, 2002: "Determinants of SGP97 Surface Soil Moisture Patterns from ESTAR and NOAH", Oral Presentation, Spring Meeting, AGU, Washington, DC, May 28-31, 2002.

Peters-Lidard, C. D., P. E. O'Neill, A. Hsu, 2002: "Determinants of SGP97 Surface Soil Moisture Patterns from ESTAR and NOAH", Poster, GAPP Mississippi River Conference, New Orleans, LA, May 13-17, 2002.

Peters-Lidard C. D., 2002. "The effects of implementing TOPMODEL concepts in the NOAH model" Oral Presentation J4.4 at the Conference on Hydrology, 82nd AMS Annual Meeting, Jan 2002, Orlando, FL, USA.

O'Neill, P., A. Hsu, E. Kim, C. Peters-Lidard, and T. England, 2001. "Performance Comparison of a Point-Scale LSP Model and the NOAH Distributed SVAT Model for Soil Moisture Estimation Using Microwave Remote Sensing," Proc. of IGARSS '01, Sydney, Australia, July 9-13, 2001.

Peters-Lidard, C., F. Pan, A. Hsu, and P. O'Neill, 2001. "ESTAR- and Model-Derived Multiscaling Characteristics of Soil Moisture during SGP97, Washita '92, and Washita '94," Proc. of IGARSS '01, Sydney, Australia, July 9-13, 2001.

Hsu, A., P. O'Neill, C. D. Peters-Lidard, and T. Jackson, 2001. "Intercomparison of Surface Soil Moisture Derived from ESTAR and Predicted by NOAH," Spring Meeting, AGU, Boston, MA, May 29-June 2, 2001.

Pan, F. and C.D. Peters-Lidard, 2001. "Downscaling and assimilating remotely sensed soil moisture data for the TOPLATS model,"Spring Meeting, AGU, Boston, MA, May 29-June 2, 2001.

Peters-Lidard, C.D., F. Pan, P.E. O'Neill, A.Y. Hsu, and P.R. Houser, 2000. "Quantifying the Relationship Between Remotely-Sensed and Modeled Soil Moisture," (abstract and poster only), GEWEX / BAHC Intl. Workshop on Soil Moisture Monitoring, Analysis, and Prediction for Hydrometeorological and Hydroclimatological Applications, Norman, OK, May 16-18, 2000, p. 27.

6. References

Chen, F., K. Mitchell, J. Schaake, Y. Xue, H. L. Pan, V. Koren, Q. .Y. Duan, M. Ek and A. Betts, 1996: Modeling of Land-Surface Evaporation by Four Schemes and Comparison with FIFE Observations. *J.Geophys. Res.* 101, 7251-7268.

Chen, F., Z. Janjic and K. Mitchell, 1997: Parameterizations in the New Land-Surface Scheme of the NCEP Mesoscale Eta Model. *Bound-Layer Meteorol.*, 85: 391-421.

Famiglietti, J. S. and E. F. Wood, 1994: Application of Multiscale Water and Energy Balance Models on a Tallgrass Prairie. *Water Resources Research*, 30(11): 3061-3078.

Houser, P. R., 1996: Remote-Sensing Soil Moisture Using Four-Dimensional Data Assimilation. Ph.D. dissertation, Department of Hydrology and Water Resources, The University of Arizona, Tucson, Arizona.

Hu, Z., Y. Chen and S. Islam, 1998: Mutiscaling properties of soil moisture images and decomposition of large- and small-scale features using wavelet transforms. *Int. J.Remote Sensing*, v19, no.13, 2451-2467.

Jackson, T. J., 1996. Southern Great Plains 1997 (SGP97) Experiment Plan, http://hydrolab.arsusda.gov/sgp97/

Jackson, T. J., and D. E. Le Vine, 1995: Mapping Surface Soil Moisture Using an Aircraft-based Passive Microwave Instrument: Algorithm and Example. *J. of Hydro.*, 184, 85-99.

Koster, R. D., and M. J. Suarez, 1996: Energy and Water Balance Calculations in the Mosaic LSM.Technical Report Series on Global Modeling and Data Assimilation, NASA Tech. Memo. 104606, Vol.9.

Mahrt, L. and H. L. Pan, 1984: A Two-LayerModel of Soil Hydrology. *Bound.-Layer Meteorol.*, 29: 1-20.

O'Neill, P., A. Hsu, T. Jackson, E. Wood, and M. Zion, 1996. Investigation of the accuracy of soil moisture inversion using microwave data and its impact on watershed hydrological modeling, Proc. of the Third Intl. Workshop on Application of Remote Sensing in Hydrology, NHRI Symposium Series, Greenbelt, MD, October 16-18, 1996, pp. 211-226.

Peters-Lidard, C. D., E. Blackburn, X. Liang and E. F. Wood, 1998: The Effect of Soil Thermal Conductivity Parameterization on Surface Energy Fluxes and Temperatures. *J. Atmos. Sci.*, 55 (7), 1209-1224.

Peters-Lidard, C. D., M. S. Zion and E. F. Wood, 1997: A Soil-Vegetation-Atmosphere Transfer Scheme for Modeling Spatially Variable Water and Energy Balance Processes, *J. Geophys. Res.*, 102 (D4), 4303-4324.

Rodriguez-Iturbe, I., G.K., Vogel, R., Rigon, D., Entekhabi, F., Castelli, and A., Rinaldo, 1995: On the spatial organization of soil moisture fields, *Geophys. Res. Letters.* v22, 2757-2760.

Rawls, W.J., D.L., Brakensick and K.E. Saxton, 1982: Estimation of soil water properties. *Trans. of the Amer. Soc. Agric. Eng.*, 25,1316-1320.

Schaake, J. C., V. I. Koren, Q. Y. Duan, K. Mitchell, and F. Chen, 1996: A Simple Water Balance Model (SWB) for Estimating Runoff at Different Spatial and Temporal Scales, *J. Geophys. Res.*, 101, 7641-7475.

Schmugge, T., T. J. Jackson, W. P. Kustas, and J. R. Wang, 1992: Passive Microwave Remote Sensing of Soil Moisture: results from HAPEX, FIFE and MONSOON 90. ISPRS *Journal of Photogrammetry and Remote Sensing*, 47:127-143.

Schmugge, T., T. J. Jackson, W. P. Kustas, R. Roberts, R. Parry, D. C. Goodrich, S. A. Amer, and M. A. Weltz, 1994: Push broom microwave radiometer observations of surface soil moisture in Monsoon '90. *Water Resources Research*, 30(5):1321-1328.